Towards mutual synchronization of serially connected Spin Torque Oscillators based on magnetic tunnel junctions

Piotr Rzeszut[a],[*] Jakub Mojsiejuk[a],[†] Witold Skowroński[a],[‡] Sumito Tsunegi[b], Hitoshi Kubota[b], and Shinji Yuasa[b]

a) AGH University of Science and Technology, Institute of Electronics,
Al. Mickiewicza 30, 30-059 Kraków, Poland
b) National Institute of Advanced Industrial Science and Technology,
Spintronics Research Center,
Tsukuba, Ibaraki 305-8568, Japan

(Dated: June 22, 2023)

Multiple neuromorphic applications require the tuning of two or more devices to a common signal. Various types of neuromorphic computation can be realized using spintronic oscillators, where the DC current induces magnetization precession, which turns into an AC voltage generator. However, in spintronics, synchronization of two oscillators using a DC signal is still a challenging problem because it requires a certain degree of similarity between devices that are to be synchronized, which may be difficult to achieve due to device parameter distribution during the fabrication process. In this work, we present experimental results on the mechanisms of synchronization of spin-torque oscillators. Devices are based on magnetic tunnel junction with a perpendicularly magnetized free layer and take advantage of a uniform magnetization precession in the presence of the magnetic field and a DC bias. By using an external microwave source, we show the optimal condition for the synchronization of the magnetic tunnel junctions. Finally, we present results on the in-series connection of two junctions and discuss the possible path towards improving oscillation power and linewidth. In addition, using numerical simulations of the coupled oscillators model, we aim to reproduce the conditions of the experiments and determine the tolerance for achieving synchronization.

I. INTRODUCTION

In recent years, neuromorphic computing concepts have gained rapid traction in multiple disciplines [1], with a promising mix of low-power and low-latency hardware-embedded algorithms. Exciting works using so-called vortex nanooscillators such as those by Romera et al.[2, 3], Torrejon et al.[4] or Tsenugi et al.[5] have also put neuromorphic concepts on the spintronics roadmap. Similar concepts of neuromorphic vowel recognition have been accomplished by spin-Hall oscillators based on nanoconstriction arrays [6]. More recently, both experimental and theoretical explorations [7] indicate that spin Hall nano oscillators can be used to construct phase-binarised Ising machines and solve some optimization problems at a potentially lower power consumption than quantum computers. Indeed, prevailing approaches have involved some type of nanooscillator where the synchronization mechanism is achieved by a combination of dipole coupling and injection locking. However, there have been some attempts to achieve coupling based on electric effects rather than magnetic ones, as explored in the work by Taniguchi [8]. Recently, Sharma et al. [9] have achieved a synchronized oscillation of up to four serially or parallel connected in-plane magnetized magnetic tunnel junctions (MTJs). Experimentally, the magnetic isolation of two devices is achieved simply by placing them further apart, so that the dipole interaction between them can be neglected (the dipole interaction decreases with distance as d^3). This usually requires an inter-device spacing of the order of μm. In this work we present an experimental study of the spin torque oscillators (STOs) realized by a magnetic tunnel junction with mixed magnetic anisotropies. To maximize the spin transfer torque acting on the free layer, an MTJ with an in-plane magnetized reference layer and a perpendicularly magnetized free layer is used. At optimal magnetic field orientation and DC bias conditions, this MTJ operates as an STO at radio frequencies with an average Q factor of 400. Using an external reference signal, we show the locking range of the STO to the half of the reference frequency, and present a study of the power dependence of in that locking range. The results of the synchronization with two MTJs connected in-series is also shown. The experiments are reproduced with numerical simulations based on coupled MTJs excited via the spin-transfer torque (STT). The Bayesian optimization allowed us to determine the magnetic parameters of the MTJ. Finally, we include a parametric study as a function of the coupling coefficient and magnetic parameters.

II. EXPERIMENTAL

A. Fabrication of MTJs

The MTJ multilayer structure is the following: *Si /SiO₂ / CMP /* (4) *Ru /* (6) *IrMn /* (2.5) *CoFe /* (0.8) *Ru /* (2.5) *CoFeB /* (1) *MgO /* (1.8) *CoFeB /* (1) *MgO /* (3) *Ru /* (5) *Ta /* (2) *Ru /* (3) *Pt* (thickness in nm). The bottom CoFeB reference layer is in-plane magnetized and is coupled to the CoFe layer, pinned to the IrMn antiferromagnet. The top CoFeB layer is characterized by a perpendicular magnetic anisotropy owing to the significant double MgO interface anisotropy contribution. The thickness of the MgO tunnel barrier corresponds to

---
[*] piotrva@agh.edu.pl
[†] mojsieju@agh.edu.pl
[‡] skowron@agh.edu.pl

the RA product of $3.6\,\Omega\,\mu m^2$.

Mixed-match three-step lithography using electron and optical lithography is performed including ion beam etching and the lift-off process to fabricate serially connected MTJs with the necessary measurement contacts (Fig. 1). The nominal dimensions of all MTJs are 130 nm in diameter, which are encapsulated in Al2O3. The resistance of a single MTJ is around67 Ω. Detailed magnetic characterization and fabrication process is described in our earlier work [10].
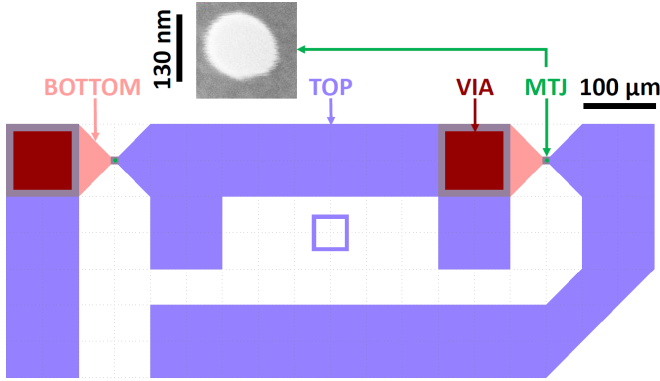

FIG. 1: Lithography mask of a single device consisting of two serially (head-to-tail) connected MTJs. Pink colour denotes a bottom electrode, red the via, violet represents the top electrode. MTJs are not visible at this scale and are fabricated on thin intersections of top and bottom electrode.

B. Measurement setup

Schematic of the measurement setup used in the experiment is presented in Fig. 2. The setup consists of an radio-frequency (RF) generator (Agilent E8257D) connected to the first symmetric port of the RP power splitter (Mini-Circuits ZN2PD2-14W-S+). The second symmetric port of the splitter is connected to the RF power amplifier (Mini-Circuits ZVA-213-S +) powered by a 12V DC power supply. The amplified signal is fed into an RF spectrum analyzer (Agilent N9030A). The combined (main) port of the power splitter is connected to an RF port of a bias tee (Mini-Circuits ZX86-12G-S+). An DC port of the bias tee is connected to the sourcemeter (Keysight B2912A). RF port of the bias tee connects to an RF probe (Picoprobe) that allows for the connection of the sample. When the RF generator was not in use it was replaced with the 50 Ω RF terminator.

The measurement system was completed with a magnetic field generator set-up, consisting of fixed electromagnet (GMW model 3472-70) powered with a current source (Kepco power supply BOP 50-20MG) and a gaussmeter (Lakeshore DSP-475) for magnetic field readout during electromagnet calibration. To change the orientation of the magnetic field vector relative to the sample plane, a dedicated rotating probe station (manufactured by Measline Ltd.) driven by a specially designed linear stepper motor driver system is used, described in [11].
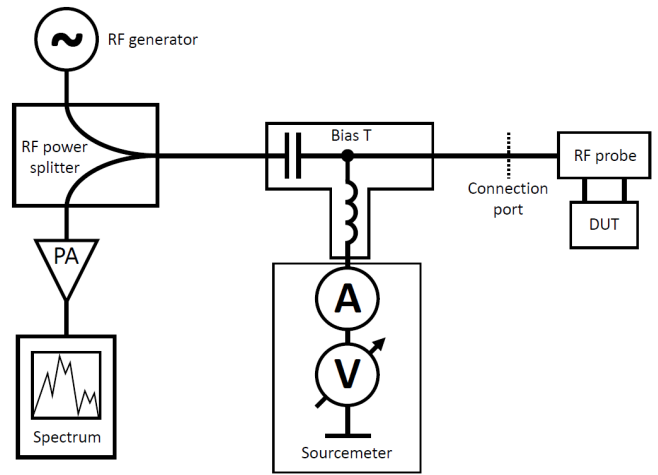

FIG. 2: Measurement setup used for injection locking experiment, utilizing directional coupler, RF generator, spectrum analyser, bias T and sourcemeter.

III. RESULTS

A. Synchronization of a single element to an external $2f$ signal

Following the procedure described in [12] we attempt to synchronize the STO with an external RF signal via the injection locking mechanism. To determine how it affects the signal parameters, we devised a setup (Fig. 2) consisting of two MTJ connected via a bias-T to a sourcemeter (which provides constant current bias) and to the RF setup: directional coupler, spectrum analyzer, and RF signal generator. As it is generally difficult to obtain an ideal impedance matching across connection between the MTJ and probe, as well as the impedance of the MTJ itself usually is different from 50 Ω. This makes observation of direct synchronization to the $1f$ signal difficult due to the significant reflection of the signal from the generator. Therefore, synchronization to the $2f$ signal might be used to investigate the synchronization of the MTJ to an external excitation and the full width at half maximum (FWHM) parameter can be used as a synchronization indicator.

The connected element was powered with a voltage of $-250\,mV$ and subjected to a magnetic field of $-120.16\,kA/m$ at spherical angles of $\theta = 25°$ relative to the normal surface vector and in-plane $\phi = 110°$ measured from the positive x axis. This resulted in a free oscillation frequency of around 4.075 GHz. Then the signal from the RF generator f_{gen} changed in the frequency range from 7.9 GHz to 8.3 GHz. The center frequency of the oscillation of STO is presented as red dots overlayed on spectra in Fig. 3 and for a range of f_{gen} values it follows the $f_{gen}/2$ frequency, which indicates that element is synchronized with the provided external $2f$ RF signal.

We calculated the FWHM for each measured point, shown in Fig. 3b). In the locking region, the FWHM significantly drops, from the average of 12.5 MHz to less than 2.5 MHz. This drop in the FWHM of the signal is another indication of
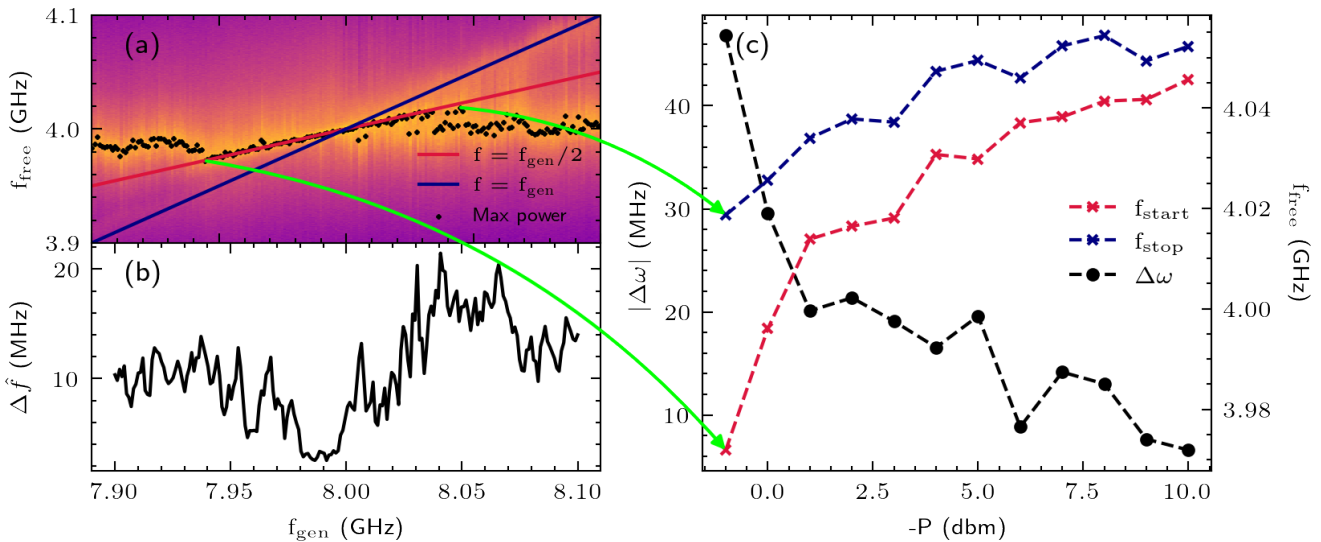
FIG. 3: (a) Power vs. frequency for different f_{gen} values. Black dots represent maximum power points, the red line denotes $f_{\text{gen}}/2$ and the dark blue one f_{gen}. (b) FWHM of the signal generated by the STO versus f_{gen}. The synchronization region is accompanied by a decrease in FWHM by a factor of 5. c) locking range $\Delta\omega$ as a function of generator power P. Note that the x-axis is in $-P$ units. As the generator power increases, the locking range increases too.

the synchronization process.

It is worth noting, that for a synchronization to occur, the experimental conditions must be very precisely controlled: the sample must me aligned precisely with an external magnetic field; the value of this magnetic field as well as DC bias require careful experimental tuning with successive approximation to achieve stable free oscillations.

B. Power levels in synchronization to an external $2f$ signal

The next step was to identify the power of the external generator, which is necessary to achieve the synchronization of the two signals. To do so, we need to take into account that power levels set on the equipment and observed during measurements are affected by the measurement setup and electrical connections. Using a vector network analyzer, the transmittance in the path from the RF signal generator to the connection port (see Fig. 2) was determined to be $-10.692\,\text{dB}$ at the representative frequency of $4.00\,\text{GHz}$. A similar measurement determined that the transmittance on the path from the connection port to the spectrum analyzer is $15.833\,\text{dB}$ at the same frequency.

The final path of the signal from the connection port to the sample is realized using an RF probe with flexible RF wires. At this point there is an impedance mismatch between the $50\,\Omega$ system and the undetermined impedance of the sample. Therefore, VNA was calibrated with an open, short and reference $50\,\Omega$ impedance (Picoprobe Calibration Substrate CS-8) connected to the RF probe and then a measurement was taken with a representative sample connected to the system. This allowed, after some standard and simple calculations, to apply

correction to all the measured power levels.

Synchronization, indicated by a decrease in FWHM, was determined to occur at injected power level delivered to the element of around $-18.740\,\text{dBm}$, while the true power generated by the element peaks at $-29.565\,\text{dBm}$.

If we wanted to employ a similar method of synchronization by using another MTJ in place of the generator, then we would find that the output signal level of the first MTJ injected into the second is below the signal level required for injection locking of the second MTJ. However, what we show below, is that the mechanism of the synchronization to $1f$ is likely more efficient than the one for $2f$.

C. Mutual synchronization of two serially connected STO

We now turn to examining two serially connected STOs, knowing that a decrease in FWHM is a good indicator of the synchronization effect. First, we collected auto-oscillation data for each element separately (indicated as left L and right R in Fig. 4), and then measured them when connected in series with a tail-to-head type connection. In all measurements, the current flowing through the elements was kept at the same value: $I_{DC} = -2.90\,\text{mA}$. For each situation FWHM we calculated and compared separate elements and their serial connection, as presented in Fig.4a). Both MTJs oscillate at similar conditions, especially at the magnetic fields below 1.6 kA/m, therefore to determine the synchronization conditions, one needs to analyze the oscillation linewidth.

It can be observed that the oscillation pattern is more complex for a serial connection than for a single element. This effect might be attributed to synchronization of the devices to
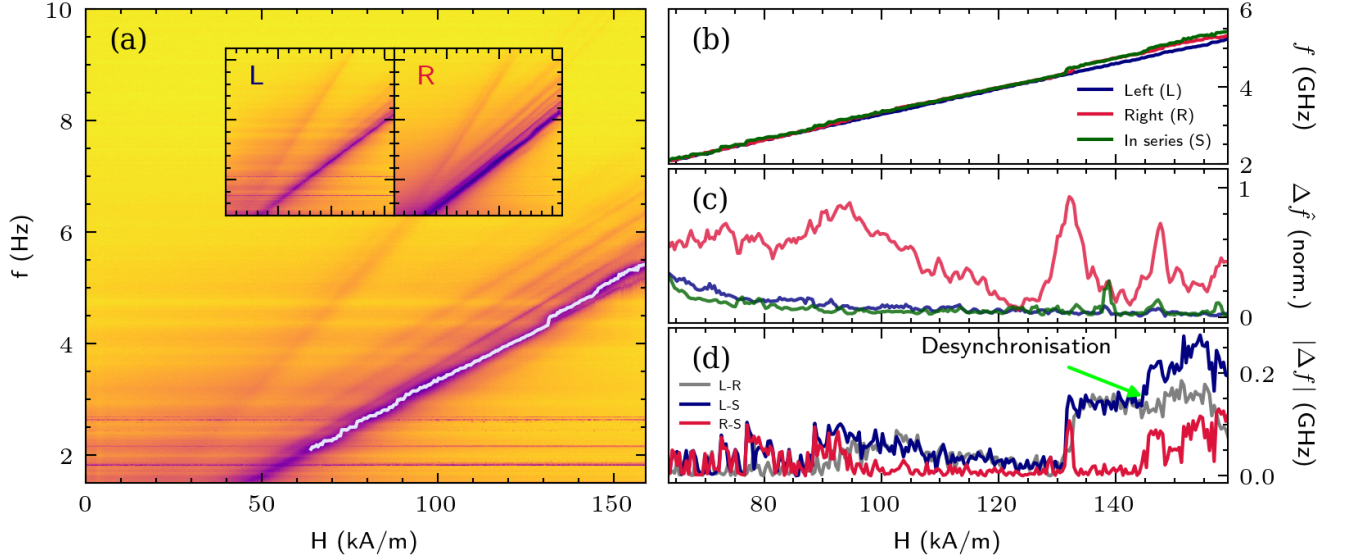
FIG. 4: Electrical synchronization and desynchronization of two serially connected MTJs. (a) In-series signal with insets illustrating separate left (L) and right (R) MTJ. The lavender-colored line designates the common resonance mode. (b) Main resonance of L, R and in-series systems. (c) FWHM of the resonance spectra and (d) the synchronization and desynchronization ranges of L and R relative to the in-series (S) signal.

each other, as we see a slight decrease in the FWHM value for some narrow conditions. The synchronization mechanism for serially connected MTJs is different from the previously presented synchronization with the $2f$ signal, as in this case we used the $1f$ frequency directly, and the change in FWHM is rather subtle as we are working in a regime of much lower powers than signal from the generator.

Fig. 4 d) reveals more information on the differences between the in series oscillation (S) and individual resonance modes of the L or R elements measured when they were not connected serially. Each line represents an absolute difference between two resonance modes from Fig.4b). Starting from about 95 kA/m we see that the line (L-R) follows the line (L-S), which means that the in-series oscillator aligns itself with one of the individual modes R measured outside the in-series connection, because (R-S) lingers near 0 during that period. This situation continues, even in the region when at approximately 132 kA/m the R and L signals begin to stray further apart from each other. In between, we observe a brief moment of nonforced synchronization in the region 125kA/m, where all signals naturally oscillate with the same frequency, also indicated by a drop in the FWHM visible in Fig.4c). Finally, beyond the 145 kA/m mark, the (L-R) line does not align with either (R-S) or (L-S). Such a pseudo-desynchronization from the R signal means that the in-series system begins to oscillate at its individual mode, different from the one enforced by R as at the lower field values. In order to get deeper insight into the mechanisms of synchronization, we performed a numerical simulations of the serially connected MTJs.

IV. NUMERICAL SIMULATIONS

For numerical simulations, we use the Landau-Lifschitz-Gilbert-Slonczewski (LLGS) macrospin equation [13–16], as implemented in the CMTJ library [17]:

$$\frac{d\mathbf{m}}{dt} = -\gamma_0 \mathbf{m} \times \mathbf{H}_{\text{eff}} + \alpha_G \mathbf{m} \times \frac{d\mathbf{m}}{dt} + f(\lambda, \eta, \mathbf{p}) \quad (1)$$

where $\mathbf{m} = \frac{\mathbf{M}}{M_s}$ is a normalized magnetization vector, with M_s as magnetization saturation, α_G as dimensionless Gilbert damping parameter, and γ_0 is the gyromagnetic factor. For our simulations, we include the spin-torque form $f(\lambda, \eta, \mathbf{p})$:

$$f(\lambda, \eta, \mathbf{p}) = -\gamma_0 \frac{\hbar j}{e\mu_0 M_s t_{\text{FM}}} \frac{\eta}{1 + \lambda \mathbf{m} \cdot \mathbf{p}} \mathbf{m} \times \mathbf{m} \times \mathbf{p} \quad (2)$$

where $\mathbf{p}$ is the vector of the normalised reference layer, η is the spin polarisation efficiency, t_{FM} as the thickness of the ferromagnetic layer (FM), j is the input current density through the reference layer, and λ is the angular parameter of the STT. In our experiments, we include the following contributions to the effective field: the demagnetization field, the anisotropy field, and the external magnetic field. Each MTJ is composed of two FM layers, where the bottom layer is set as a reference layer for the top layer, which accounts for the STT modeling.

A. Finding the MTJ parameters

To adequately reproduce the fabrication parameters, we perform Bayesian optimization with respect to the maximum

Parameter	Value	Unit
$M_{s,1}$	0.92	T
$M_{s,2}$	1.21	
$K_{u,1}$	0.31	MJ/m³
$K_{u,2}$	6.35	

TABLE I: Parameters obtained from running the Bayesian optimisation on the single junction.

resonance lines obtained from the auto-oscillation spectra under DC. In this procedure, we find the optimal parameters for one of the junctions in the pair. We designed a macrospin simulation using the CMTJ package [17] where we sweep with the external magnetic field in the range [0, 160] kA/m, at the polar angle $\theta = 5°$ and the azimuth angle $\phi = 90°$. At each step, we apply a constant current density, equivalent to feeding 1.5mA perpendicularly through the junction. We assumed the perpendicular anisotropy of the top layer and the in-plane anisotropy of the bottom layer. The IEC energy is assumed to be negligible in our experiments. In the next step, we run the Bayesian optimisation algorithm with a mean squared error (MSE) cost function:

$$\text{MSE} = \sum_i (f_i - \bar{f}_i)^2 \quad (3)$$

where the index i iterates over steps of the applied field, f_i is the experimental frequency measured at H_i and $\bar{f}_i$ is the simulated frequency at H_i under the set of parameters currently considered. Due to the multiplicity of proximate solutions [18], it is necessary to limit the design space with a set of the boundaries, thus we seed the optimization process with a boundary condition in the approximate range of reasonable values of M_s and K_u (uniaxial anisotropy constant) for each layer. In our procedures, we used the Python package for Bayesian optimization [19]. Shortly, Bayesian optimisation relies on optimising the acquisition function u over a Gaussian process [20, 21], such that:

$$\hat{\theta} = \underset{\theta}{\text{argmax}} \; u(\theta|\mathscr{D}) \quad (4)$$

where $\mathscr{D}$ is the resonance frequency data, θ are the MTJ parameters to optimise, and $\hat{\theta}$ are the best-fit parameters. The successive suggestions are sourced by evaluating the acquisition function with some added noise. The starting prior is usually chosen as a uniform distribution. We use the upper confidence bound (UCB) algorithm as the acquisition function and run the optimization for 500-1000 steps.

As a result of running the optimization, we obtain an approximate local minimal solution of the saturation magnetization $M_{s,1}$, $M_{s,2}$ and magnetic anisotropy energies $K_{u,1}$, $K_{u,2}$, with final values summarized in Tab.I (the numerical subscript indicates the layer index, 1 denotes free and 2, the reference layer). Fig.5 presents an example auto-oscillation spectrum with the solid line representing the experimentally measured maximum amplitude resonance line.
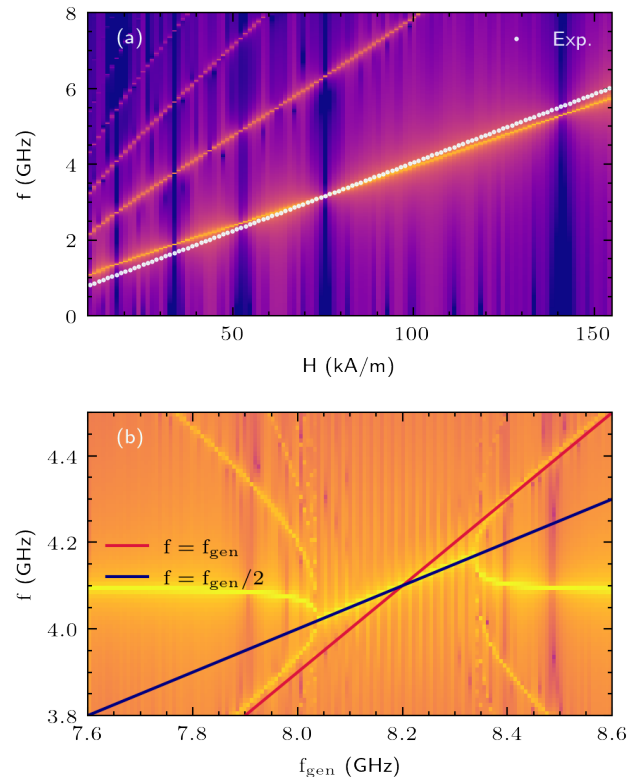

FIG. 5: a) The spectrum computed from the parameters obtained during Bayesian optimisation procedure for a single MTJ. Dotted white line represents the experimental main harmonic resonance line. The precise parameter values have been placed in Tab.I. b) simulated injection locking with $\Delta j_{AC}/j_{DC} \approx 0.2$.

B. Model of synchronization

A theory of synchronization of a single MTJ follows an auto-oscillator theory developed in [22]. First, we attempt to obtain the phenomenon of injection locking at a frequency $2f$, where f is the natural frequency of an MTJ in a given field H_{ext} and j_{dc}. Locking to the $2f$ frequency instead of f has the experimental advantage of removing the crosstalk from the generator. We find a ratio $\Delta j_{ac}/j_{dc}$ between 0.1 and 0.2 sufficient to achieve injection lock. The results of simulated injection locking are depicted in Fig.5b). The MTJ oscillations snap to $f_{gen}/2$ of the locking signal, as illustrated by the change of slope within the synchronization range.

We enforce the synchronization behavior of electrically coupled MTJs after Taniguchi et al. [8]. We assume that two oscillators are sufficiently far apart so that there is no dipole interaction between them. There are two available configurations for connecting two MTJs, serial and parallel, and in this work we only consider the former. In each, the current depends on the free magnetizations **m** and the reference layers **p**
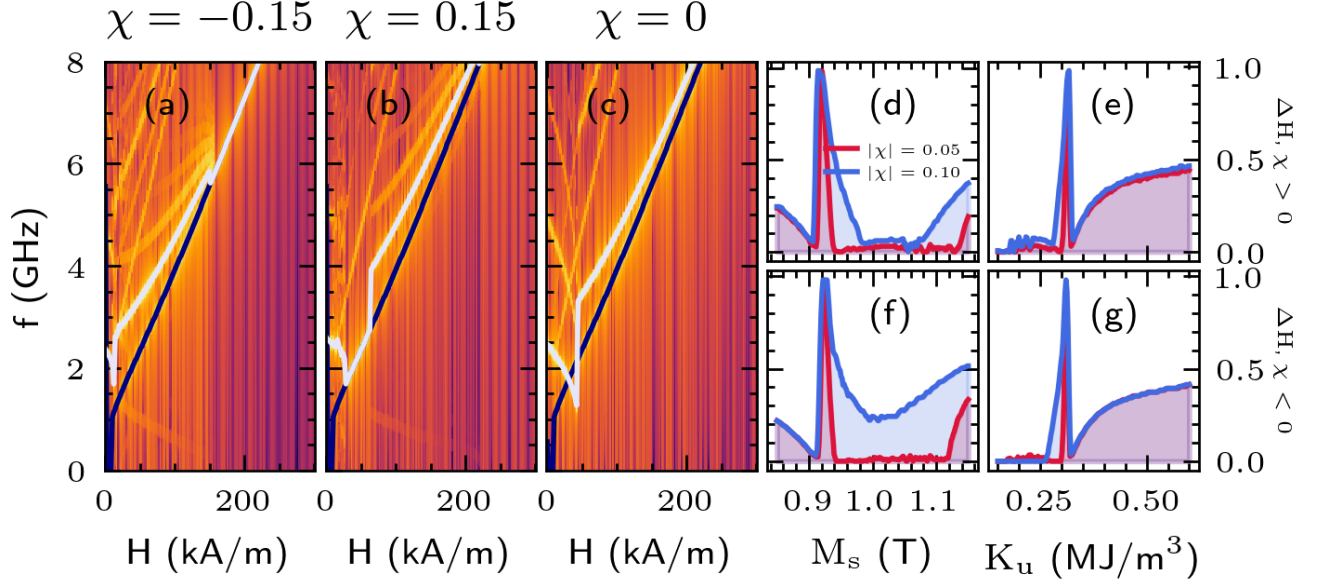
FIG. 6: An example of in-series synchronization and desynchronization of two MTJs. (a-c) negative, positive, and null values of χ, the coupling constant. We can observe that two MTJs begin to synchronize above 125 kA/m in case of negative χ(a) and between 40 and 75 kA/m for a positive χ (B). The dark blue and azure colors in the third panel (c) show the individual resonance modes of MTJs while they are excited with an equal current density before being connected in series. (d-g) Normalized mutual locking ranges ΔH for four values of the coupling constant: d-e) positive and e-g) negative χ, respectively, calculated for a range of $M_{s,2}$ and $K_{u,2}$ values. Red lines denote $|\chi| = 0.05$ and blue lines $|\chi| = 0.1$.

of the junctions i_{th} and $i+1_{th}$:

$$I(t) = I_0(t) + \chi I_0(t)(\mathbf{m_i} \cdot \mathbf{p}_i + \mathbf{m}_{i+1} \cdot \mathbf{p}_{i+1}) \quad \text{(series)} \quad (5)$$
$$I(t) = I_0(t) + \chi I_0(t)(\mathbf{m_i} \cdot \mathbf{p}_i - \mathbf{m}_{i+1} \cdot \mathbf{p}_{i+1}) \quad \text{(parallel)} \quad (6)$$

where $I_0(t)$ is the value of the current fed into the first MTJ in the connection and χ is the unitless coupling strength. We show an example of synchronization in Fig.6. The first of two serially connected MTJs was created with the parameters derived from the Bayesian fitting procedure in the preceding section, while the other had each of its parameters initialized from a normal distribution centered on the original MTJ parameter value, with a standard deviation of δ. The applied external magnetic field is 300 kAm/m, at $(\theta, \phi) = (15, 90)$ and the system was excited with a constant current density of 36.7 GA/m^2. In addition, we conducted parametric simulations for the locking ranges ΔH for a range of values of $M_{s,2}$ and $K_{u,2}$ of the second junction of the in-series connection. Upon varying either of the parameters, all remaining values are given as in Tab.I. When the absolute value of χ increases, we observe a widening of the peaks and a clear expansion of the locking range over a larger scale of the parameter variation, most evident in Fig.6f). Interestingly, that increase in χ has a larger impact on the tolerance of the M_s parameter than on the anisotropy energy. The drift towards larger values of the parameter in all figures suggests the secondary harmonic synchronization phenomenon (the natural frequency of the second MTJ naturally increases as either of the parameters increases).

V. DISCUSSION

Achieving electric synchronization with spin-torque oscillators requires a great level of precision and tedious tuning of the junction parameters. Apart from the difficulty in orchestrating the correct setup, specific synchronization ranges depend largely on the relative parameter dispersion. Based on the experimental approach, we were able to present the oscillations in individual STOs and in serially connected pair of MTJs. Finally, we note that the desynchronization, i.e. relative drift of the individual modes from the common mode, can be both measured experimentally and modeled with a relatively simple model. Simulation results suggest that the parallel connection of the STOs may lead to improved synchronization, however without possibility of determining the performance of individual elements. Joint experimental and numerical methodology established in this work allows for inspecting individual MTJs separately and then measuring the resonance spectrum of the same pair in a in-series connection. Such an inductive approach facilitates numerical modelling and as a result may give deeper insight into the operation conditions of the system as a whole. One method to achieve reliable locking of two MTJs in the same mode may be to connect more devices together, creating less selective circuits with broader bandwidths. Developing such a method can lead to promising opportunities for creating arrays of tunable oscillators capable of performing simple computing tasks.

[1] K. Roy, A. Jaiswal, and P. Panda, Towards spike-based machine intelligence with neuromorphic computing, Nature **575**, 607 (2019).

[2] M. Romera, P. Talatchian, S. Tsunegi, F. Abreu Araujo, V. Cros, P. Bortolotti, J. Trastoy, K. Yakushiji, A. Fukushima, H. Kubota, S. Yuasa, M. Ernoult, D. Vodenicarevic, T. Hirtzlin, N. Locatelli, D. Querlioz, and J. Grollier, Vowel recognition with four coupled spin-torque nano-oscillators, Nature **563**, 230 (2018).

[3] M. Romera, P. Talatchian, S. Tsunegi, K. Yakushiji, A. Fukushima, H. Kubota, S. Yuasa, V. Cros, P. Bortolotti, M. Ernoult, D. Querlioz, and J. Grollier, Binding events through the mutual synchronization of spintronic nano-neurons, Nat. Commun. **13**, 883 (2022).

[4] J. Torrejon, M. Riou, F. A. Araujo, S. Tsunegi, G. Khalsa, D. Querlioz, P. Bortolotti, V. Cros, K. Yakushiji, A. Fukushima, H. Kubota, S. Yuasa, M. D. Stiles, and J. Grollier, Neuromorphic computing with nanoscale spintronic oscillators, Nature **547**, 428 (2017).

[5] S. Tsunegi, T. Taniguchi, R. Lebrun, K. Yakushiji, V. Cros, J. Grollier, A. Fukushima, S. Yuasa, and H. Kubota, Scaling up electrically synchronized spin torque oscillator networks, Sci. Rep. **8**, 13475 (2018).

[6] M. Zahedinejad, A. A. Awad, S. Muralidhar, R. Khymyn, H. Fulara, H. Mazraati, M. Dvornik, and J. Åkerman, Two-dimensional mutually synchronized spin Hall nano-oscillator arrays for neuromorphic computing, Nature Nanotechnology **15**, 47 (2020).

[7] A. Houshang, M. Zahedinejad, S. Muralidhar, J. Chęciński, R. Khymyn, M. Rajabali, H. Fulara, A. A. Awad, M. Dvornik, and J. Åkerman, Phase-Binarized Spin Hall Nano-Oscillator Arrays: Towards Spin Hall Ising Machines, Phys. Rev. Appl. **17**, 014003 (2022).

[8] T. Taniguchi, Synchronization and chaos in spin torque oscillator with two free layers, AIP Adv. **10**, 015112 (2020).

[9] R. Sharma, R. Mishra, T. Ngo, Y.-X. Guo, S. Fukami, H. Sato, H. Ohno, and H. Yang, Electrically connected spin-torque oscillators array for 2.4 GHz WiFi band transmission and energy harvesting, Nat. Commun. **12**, 2924 (2021).

[10] W. Skowroński, J. Chęciński, S. Ziętek, K. Yakushiji, and S. Yuasa, Microwave magnetic field modulation of spin torque oscillator based on perpendicular magnetic tunnel junctions, Sci. Rep. **9**, 19091 (2019).

[11] W. Skowroński, K. Grochot, P. Rzeszut, S. Łazarski, G. Gajoch, C. Worek, J. Kanak, T. Stobiecki, J. Langer, B. Ocker, and M. Vafaee, Angular Harmonic Hall Voltage and Magnetoresistance Measurements of Pt/FeCoB and Pt-Ti/FeCoB Bilayers for Spin Hall Conductivity Determination, IEEE Transactions on Electron Devices **68**, 6379 (2021).

[12] M. Quinsat, J. F. Sierra, I. Firastrau, V. Tiberkevich, A. Slavin, D. Gusakova, L. D. Buda-Prejbeanu, M. Zarudniev, J.-P. Michel, U. Ebels, B. Dieny, M.-C. Cyrille, J. A. Katine, D. Mauri, and A. Zeltser, Injection locking of tunnel junction oscillators to a microwave current, Applied Physics Letters **98**, 182503 (2011).

[13] T. Gilbert, Classics in Magnetics A Phenomenological Theory of Damping in Ferromagnetic Materials, IEEE Transactions on Magnetics **40**, 3443 (2004).

[14] D. Ralph and M. Stiles, Spin transfer torques, J. Magn. Magn. Mater. **320**, 1190 (2008).

[15] J. Slonczewski, Current-driven excitation of magnetic multilayers, Journal of Magnetism and Magnetic Materials **159**, L1 (1996).

[16] J. Slonczewski, Currents and torques in metallic magnetic multilayers, J. Magn. Magn. Mater. **247**, 324 (2002).

[17] J. Mojsiejuk, S. Ziętek, K. Grochot, W. Skowroński, and T. Stobiecki, cmtj: Simulation package for analysis of multilayer spintronic devices, npj Computational Materials **9**, 54 (2023).

[18] S. Ziętek, J. Mojsiejuk, K. Grochot, S. Łazarski, W. Skowroński, and T. Stobiecki, Numerical model of harmonic Hall voltage detection for spintronic devices, Physical Review B **106**, 024403 (2022).

[19] fernando, Bayesian Optimization (2022), original-date: 2014-06-06T08:18:56Z.

[20] E. Brochu, V. M. Cora, and N. de Freitas, *A Tutorial on Bayesian Optimization of Expensive Cost Functions, with Application to Active User Modeling and Hierarchical Reinforcement Learning*, Tech. Rep. arXiv:1012.2599 (arXiv, 2010) arXiv:1012.2599 [cs] version: 1 type: article.

[21] J. Snoek, H. Larochelle, and R. P. Adams, Practical Bayesian Optimization of Machine Learning Algorithms, in *Advances in Neural Information Processing Systems*, Vol. 25 (Curran Associates, Inc., 2012).

[22] A. Slavin and V. Tiberkevich, Nonlinear Auto-Oscillator Theory of Microwave Generation by Spin-Polarized Current, IEEE Transactions on Magnetics **45**, 1875 (2009).